Electronic Supplementary Material (ESI) for Energy & Environmental Science.

Electronic Supplementary Information

Boosted Charge Extraction of NbO_x-Enveloped SnO_2 Nanocrystals Enable 24% Efficient Planar Perovskite Solar Cells

Ruihan Yuan,‡[a] Bing Cai,‡[a] Yinhua Lv ,*[a] Xiang Gao,[b] Jinwen Gu,[c] Zhenghui Fan,[a] Xinhang Liu,[a] Chi Yang,[d] Mingzhen Liu*[c] and Wen-Hua Zhang *[a]

[a] Sichuan Research Center of New Materials, Institute of Chemical Materials, China Academy of Engineering Physics, 596 Yinhe Road, Shuangliu, Chengdu 610200, China. E-mail: qiehahah@163.com; whzhang@caep.cn

[b] Center for High Pressure Science & Technology Advanced Research, 10 Xibeiwang East Road, Haidian District, Beijing 100094, P.R. China.

[c] School of Materials and Energy, University of Electronic Science and Technology of China, Chengdu 611731, P.R. China. E-mail: mingzhen.liu@uestc.edu.cn

[d] Institute for Advanced Study, Chengdu University, 2025 Chengluo Avenue, Chengdu, 610106, China.

‡ These authors contributed equally to this work.

* Corresponding author.

Experimental Procedures

Materials. All of the solvents and reagents were used as received without further purification. Tin (IV) chloride pentahydrate ($SnCl_4 \cdot 5H_2O$, 99.0%), HAc (AR) and Ammonia solution (AR) were purchased from Sinopharm Chemical Reagent Co. Ltd. Concentrated HCl (36.5-38 wt%, GR) were purchased from Xilong Scientific Co. Ltd. Niobium(V) chloride (99.9%) was purchased from Alfa Aesar Co. Ltd. Ethanol (99.5%), and EG (99%) were purchased from Aladdin Reagent Co. Ltd. PbI_2 was bought from TCI Co. Ltd. FAI, MABr, MACl, CsI, and 2,2',7,7'-tetrakis[N,N-di(4-methoxyphenyl)amino]-9,9'-spirobifluorene (Sprio-OMeTAD) were all purchased from Xi'an Polymer Light Technology Corp. Li-TFSI, 4-tert-butylpyridine (tBP), N, N- dimethyl methanamide (DMF) and dimethyl sulfoxide (DMSO) were purchased from Sigma Aldrich. The indium tin oxide (ITO) glass is a commercial product from South China Science and Technology Company Limited (China). The polyethylene naphthalate (PEN)/ITO was purchased from Advanced Election Technology Co. Ltd.

Preparation of the SnO_2 NCs. SnO_2 NCs were prepared according to a modified method.[1] Typically, 5 g of $SnCl_4 \cdot 5H_2O$ was first dissolved in 50 mL of EG and stirred overnight. Then 10 mL of the above solution was pipetted into a round-bottomed flask, and 2 mL of HAc and ammonia solution were added into it under stirring. After cooling down to room temperature, the round-bottomed flask was placed in an oil bath and heated for tens of minutes at 150 ˚C. Then the solution was centrifuged with ethanol at 2500 rpm for twice and 5000 rpm for twice. Finally, the centrifuge products were dispersed into 30 mL of ethanol to form a SnO_2 NC dispersed solution with a concentration of 13 mg/mL.

Preparation of "Enveloped" SnO_2 (SnO_2/NbO_x). 2 mL of SnO_2 NCs-ethanol solution was added into 8 mL of $NbCl_5$ solution (0.02 M aqueous solution with 0.5 mL of HCl). After mixing well, the beaker was placed in an oil bath and heated for varied reaction time at 70 ˚C. Then the solution was centrifuged with ethanol at 3500 rpm for twice. The centrifuge products were dispersed into 5 mL ethanol and the solution was dispersed by ultrasound machine before use.

Device Fabrication. The ITO glass substrates and PEN/ITO flexible substrates were sequentially cleaned with water and ethanol. The SnO_2 NCs and SnO_2/NbO_x films were fabricated by spin coating their corresponding dispersions machine at 2000 rpm with an acceleration of 2000 rpm/s, and annealed at 150 ˚C for 30 minutes (for the flexible substrates, the annealing temperature was 100 ˚C). After cooling down to room temperature, the substrates were treated with UV-O for 15 min before use. The perovskite films were prepared via a two-step spin-coating method.[2] 1.5 M of PbI_2 in DMF: DMSO solution (9:1, v/v) was spin-coated onto SnO_2 NCs or SnO_2/NbO_x substrates at 1500 rpm for 30 s to form a yellow PbI_2-DMSO film and heated at 70 ˚C for 10 s. After cooled down to room temperature, 0.05 mL of 2-propanol solution containing 90 mg of FAI, 6.36 mg of MAI and 9 mg of MACl, was spin-coated atop PbI_2-DMSO film at 2000 rpm for 30 s. Then the films annealed on a hot plate at 150 ˚C for 20 min in ambient air conditions (for the flexible substrates, the heating temperature was 120 ˚C). After cooling down to room temperature, the hole transport material solution was spin coated onto perovskite films at 4500 rpm for 30 s, which was consisted with 72.3 mg Spiro-OMeTAD, 28.8 µL 4-tert-butylpyridine, 17.5 µL Li-TFSI/acetonitrile (520 mg/mL), and 1 mL chlorobenzene. Finally, 80 nm of gold top electrode was thermally evaporated under high vacuum.

Characterizations. Photovoltaic performance of solar cell devices was measured under illumination of a simulated sunlight (AM 1.5, 100 mW/cm^2, SSF5-3A, Enlitech), and the *J-V* curves were recorded using a Keithley digital source meter (Model 2400). The active area of the solar cells was confirmed by using a metal aperture of 0.09 cm^2 to avoid light scattering through the sides. The external quantum efficiencies were measured in AC mode by a QE-R3011 testing system (Enlitech). The PL measurement was performed with time-correlated single photon counting (TCSPC) with a 510 nm laser (DD-510L, Deltaflex, Horiba). An Keysight Technologies 7500 (AFM) was used to obtain surface RMS roughness of SnO_2 NCs, SnO_2/NbO_x, and perovskite films. X-ray diffraction (XRD) patterns were recorded by a D8 X-ray diffractometer (X' pert Pro-1), employing Cu K_α as incident radiation. The morphologies of the samples were obtained by scanning electron microscopy (Hitachi S5200 and Sigma HD, Zeiss) and transmission electron microscope (TEM; JEOL, JEM-2100, 200 KV). The absorption and transmission were checked by a UV–VIS spectrophotometer (Evolution^{TM} 201, Thermo fisher scientific Corporation). The XPS result was obtained by Thermo ESCALAB 250Xi. The energy band structure of samples was evaluated by an ultraviolet photoemission spectroscopy (UPS) (Thermo Scientific, Escalab 250Xi). The linear sweep voltammetry, electrochemical impedance, admittance spectroscopy measurement and Mott-Schottky analysis were conducted by using a multi-channel potentiometer (VMP3, Biologic). During the Mott-Schottky measurement, the electrodes were submerged in a 0.1 M NaCl aqueous solution, with a Pt and Ag/AgCl as counter and reference electrode, respectively. The values were recorded at frequency of 80 mHz. EIS data were recorded from 0 to 0.6 V in the frequency range from 1 MHz to 100 mHz with an AC amplitude of 10 mV. The Mott-Schottky data were recorded at the frequency of 50 KHz in the applied voltage range from -1.5 V to 0 V with an AC amplitude of 25 mV. IMPS/IMVS methods were performed using an impedance analyzer (Modulab XM, Solartron Metrology) under illumination (yellow-emitting LED, λ = 590 nm). The mean transport (τ_{ct}) and recombination times (τ_r) of the photogenerated charges were obtained from the IMVS/IMPS curves by setting $\tau = 1/2\pi f_{min}$ (IMPS, IMVS), respectively. The contact angel test was conducted by using Contact Angle measuring instrument (Dataphysics OCA50), and the solvent used for the test was PbI_2-precursor solution (DMF/DMSO, 9:1, v/v). For the light soaking stability test, unencapsulated PSCs were placed in a N_2-filled glove box under one sun irradiation at the open circuit condition. The chamber atmosphere temperature is controlled at 30±5 ℃.

Explanation of the movies. Movies 1 and 2 display the contact angels test results of PbI_2 precusor solution on the SnO_2/NbO_x, SnO_2 NCs film substates.

Supplementary figures and tables

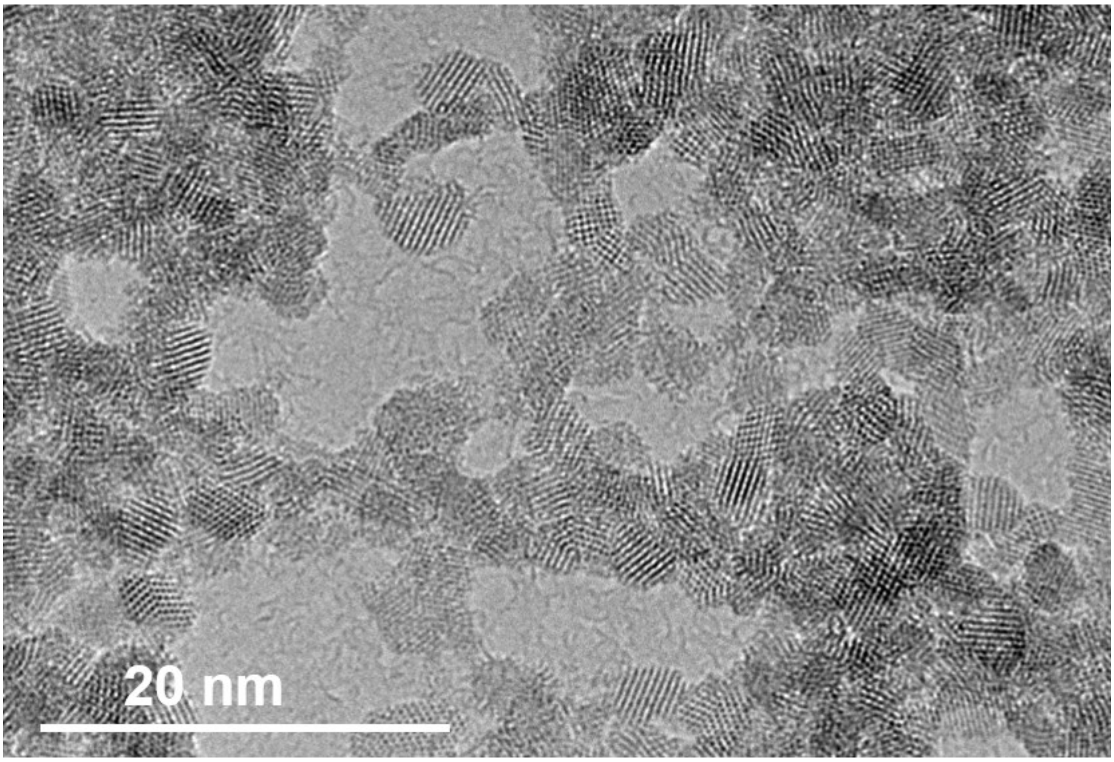

Figure S1. The TEM image of SnO_2 NCs.

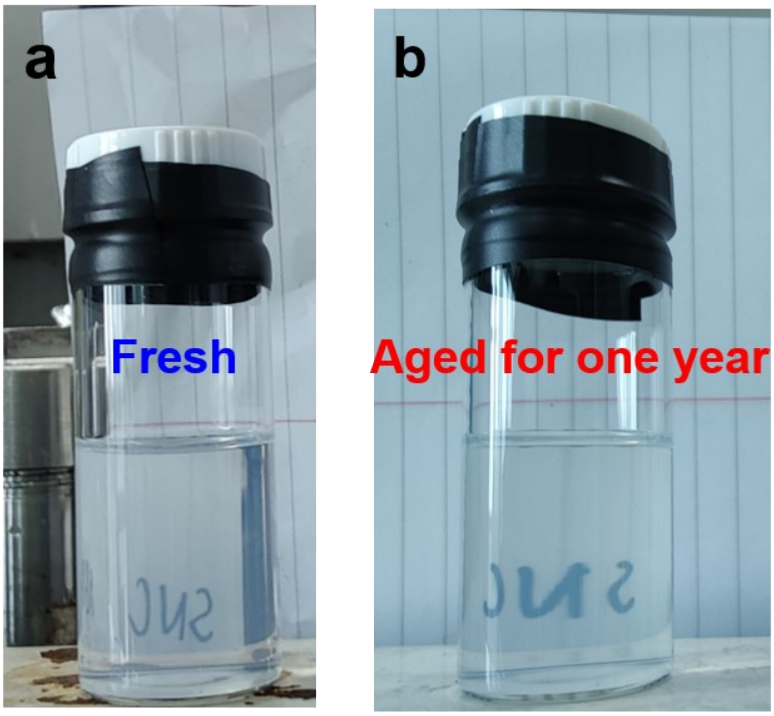

Figure S2. The digital photos of the fresh (a) and aged (b) SnO_2 NC dispersion solutions (concentration of 13 mg/mL) in a refrigerator for one year.

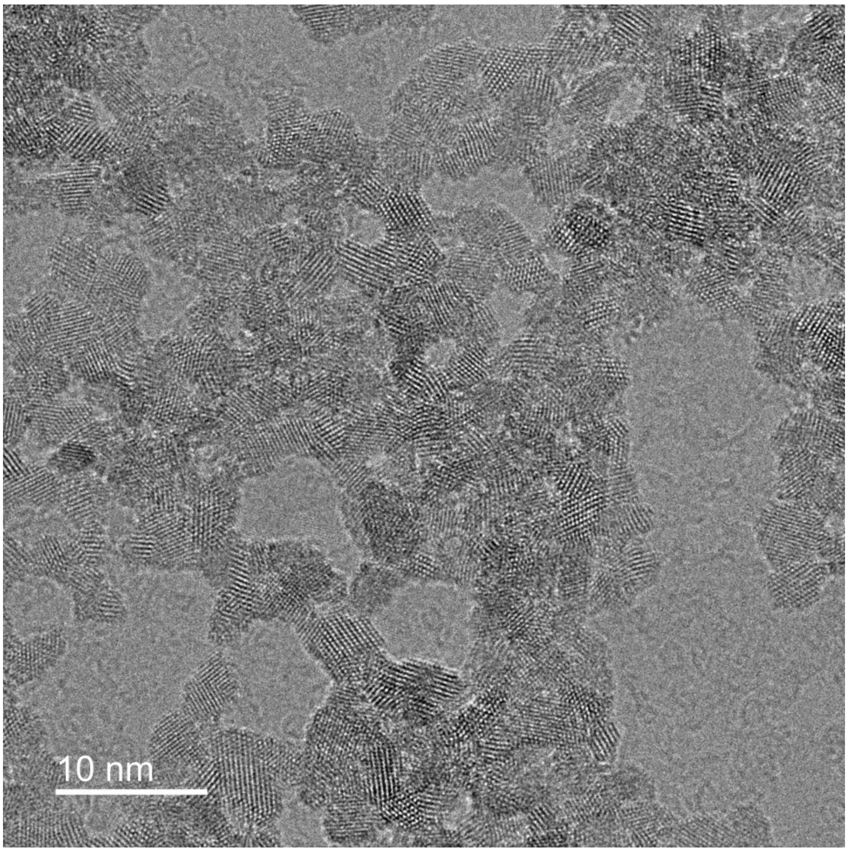

Figure S3. The HRTEM images of SnO_2 NCs aged in a refrigerator for one year.

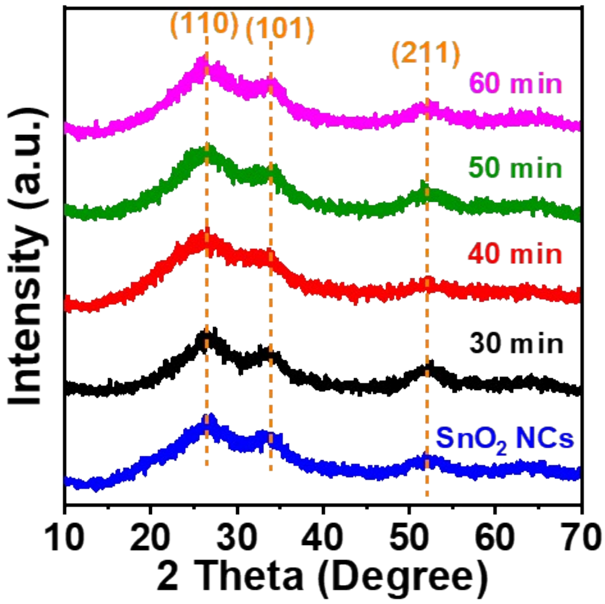

Figure S4. XRD patterns of SnO_2 and SnO_2/NbO_x NCs with different growth time of NbO_x.

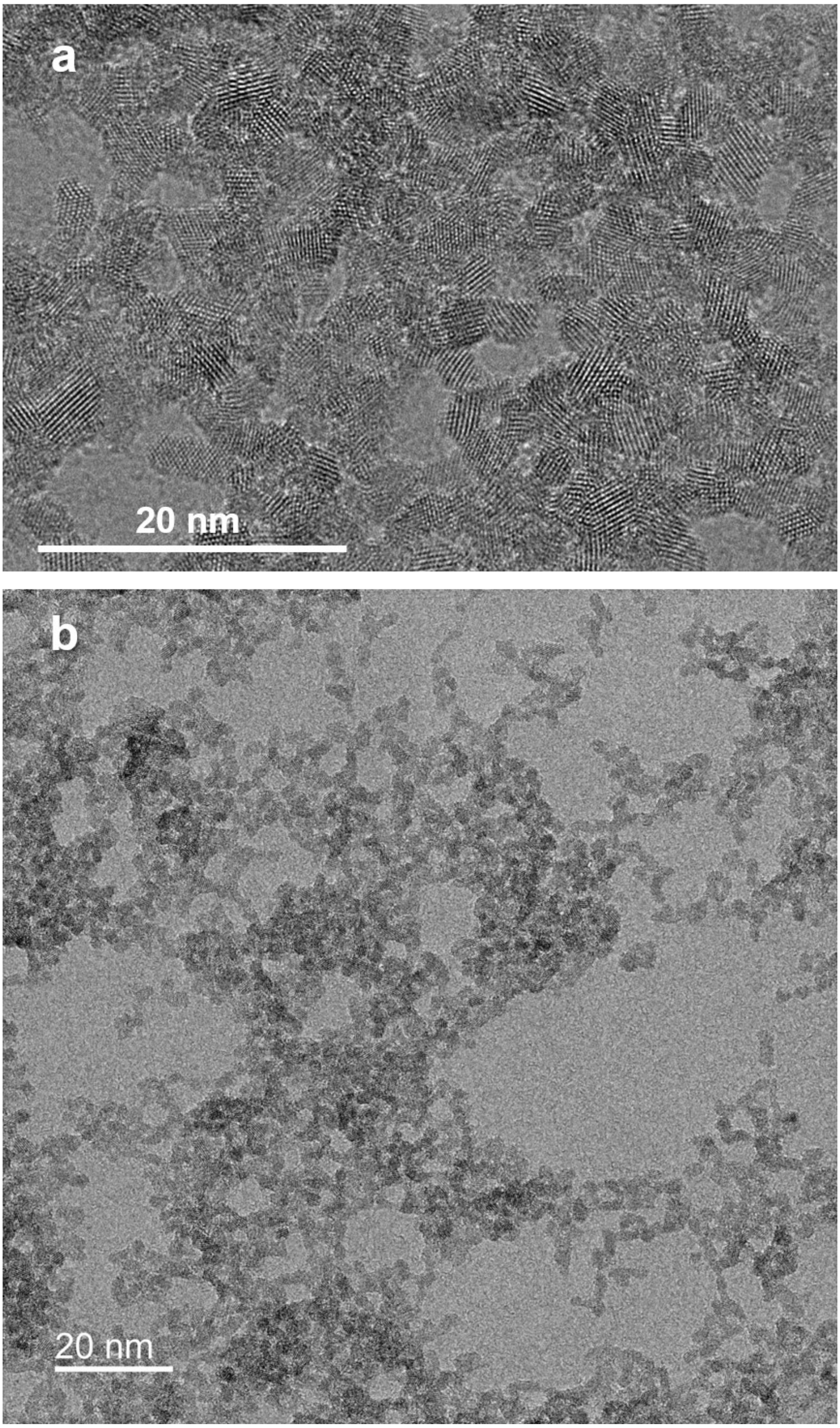

Figure S5. The TEM images of the SnO_2/NbO_x NCs.

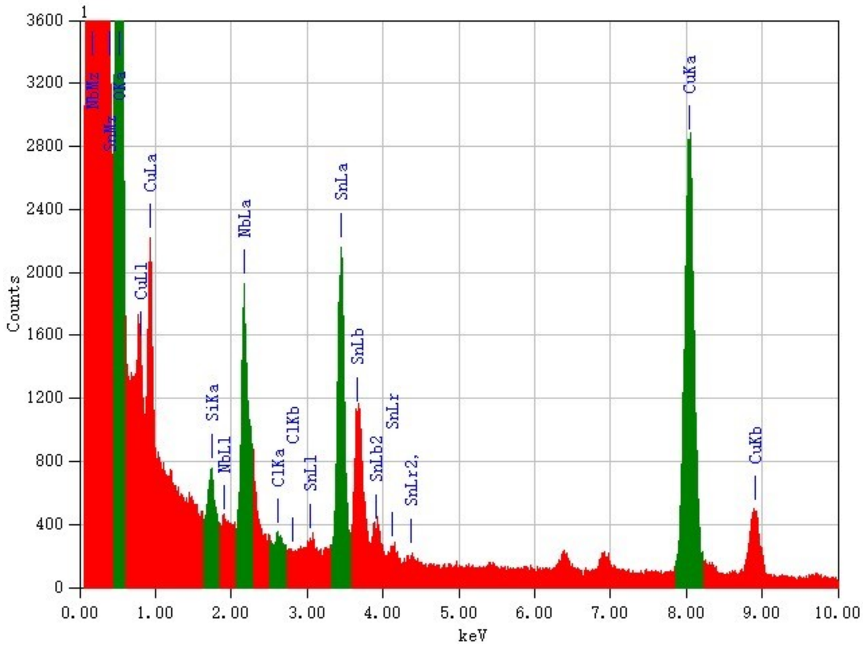

Figure S6. The EDX spectrum of SnO_2/NbO_x NCs.

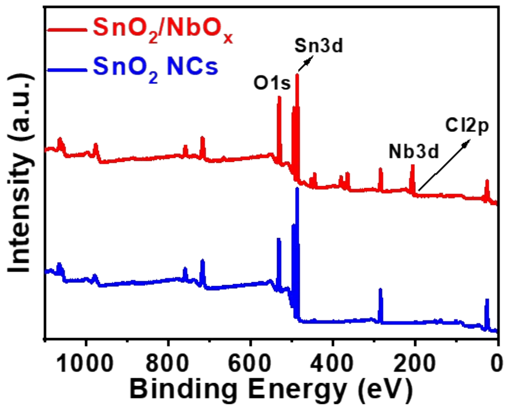

Figure S7. The XPS survey spectra of the SnO_2 and SnO_2/NbO_x NCs.

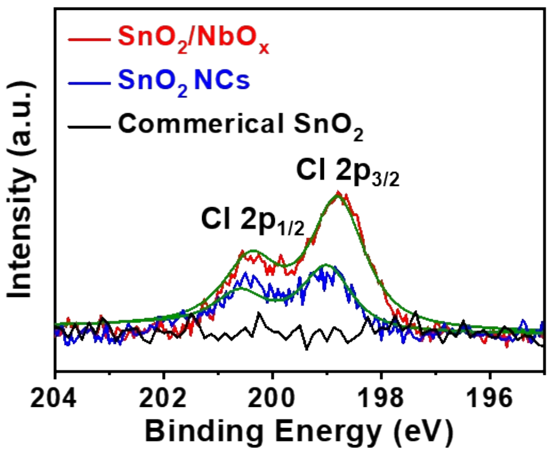

Figure S8. The high-resolution XPS spectra of Cl 2p of Commerical SnO_2, SnO_2 NCs, and SnO_2/NbO_x NCs.

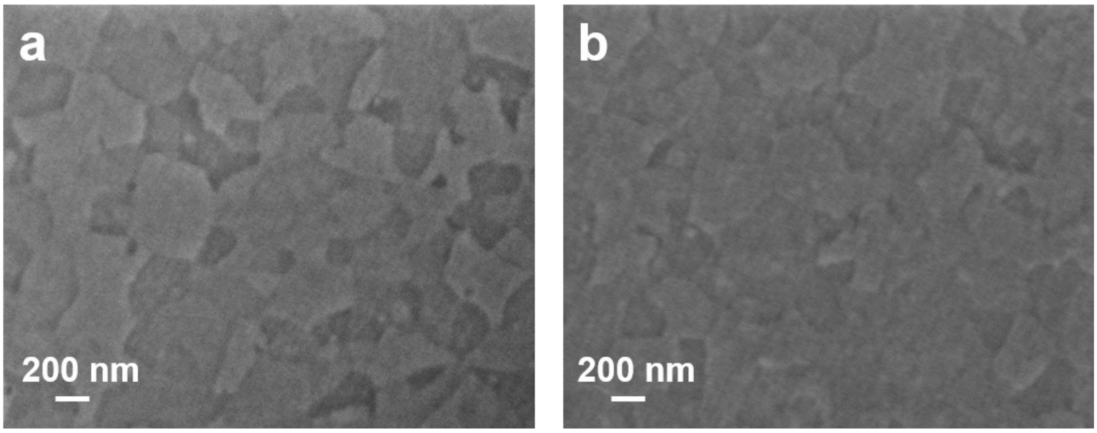

Figure S9. The SEM images of compact films on ITO substrates: (a) SnO_2 and (b) SnO_2/NbO_x NCs.

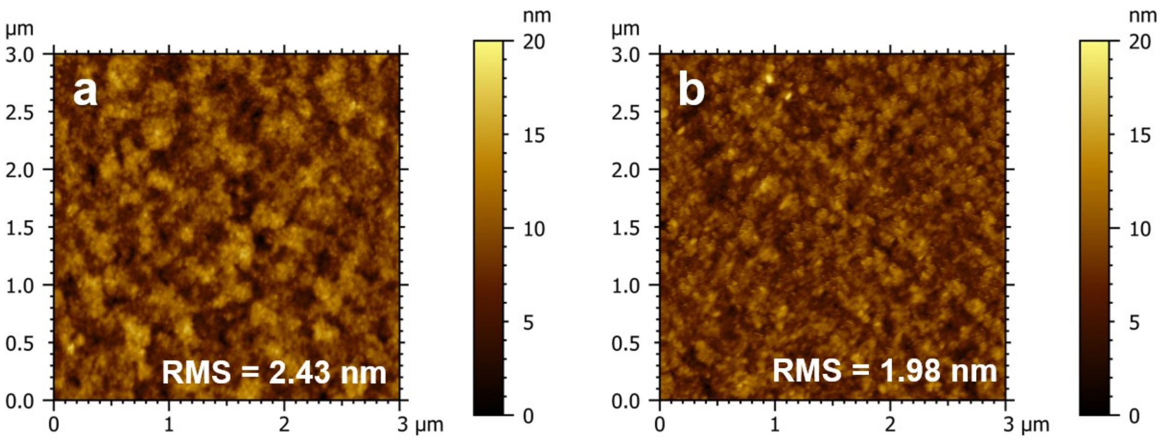

Figure S10. The AFM images of compact films on ITO substrates: (a) SnO_2 and (b) SnO_2/NbO_x NCs.

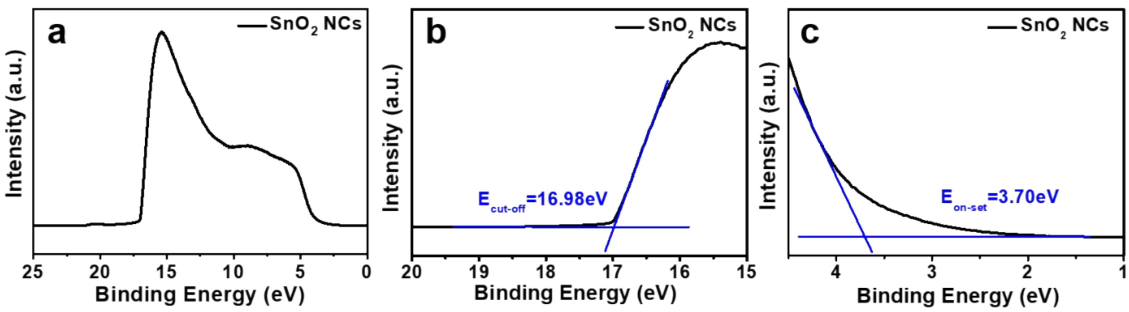

Figure S11. The UPS spectra of SnO_2 NCs: (a) full range, (b) cut-off energies ($E_{cut\text{-}off}$), and (c) on-set energies ($E_{on\text{-}set}$).

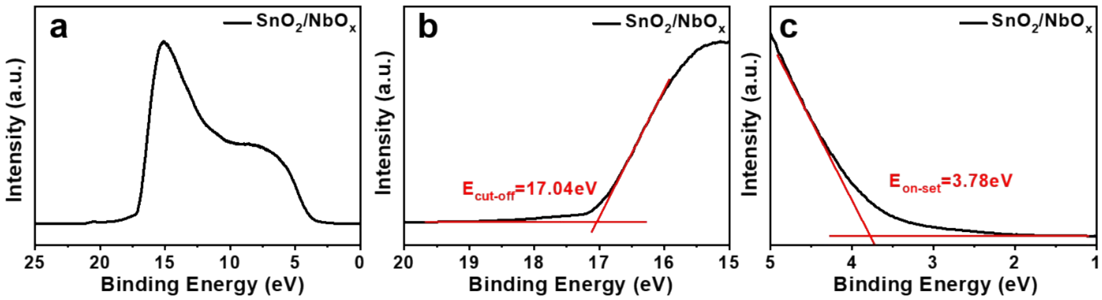

Figure S12. The UPS spectra of SnO_2/NbO_x NCs: (a) full range, (b) cut-off energies ($E_{cut\text{-}off}$), and (c) on-set energies ($E_{on\text{-}set}$).

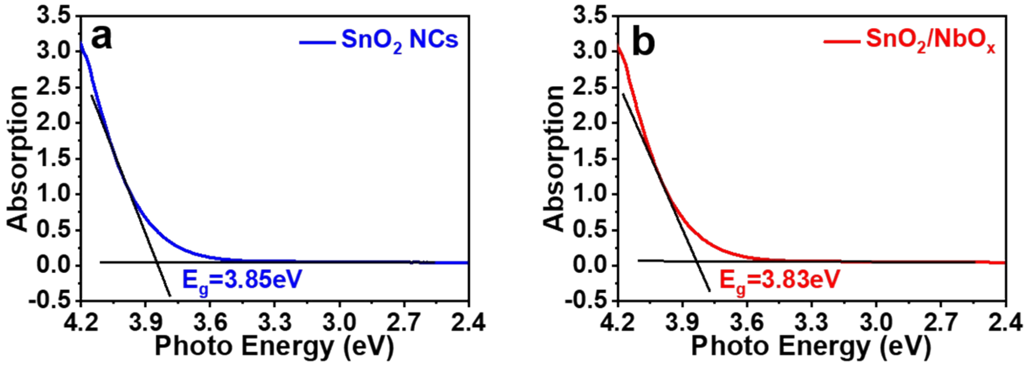

Figure S13. The UV-Vis absorption spectra of compact films on ITO substrates: (a) SnO_2 and (b) SnO_2/NbO_x NCs.

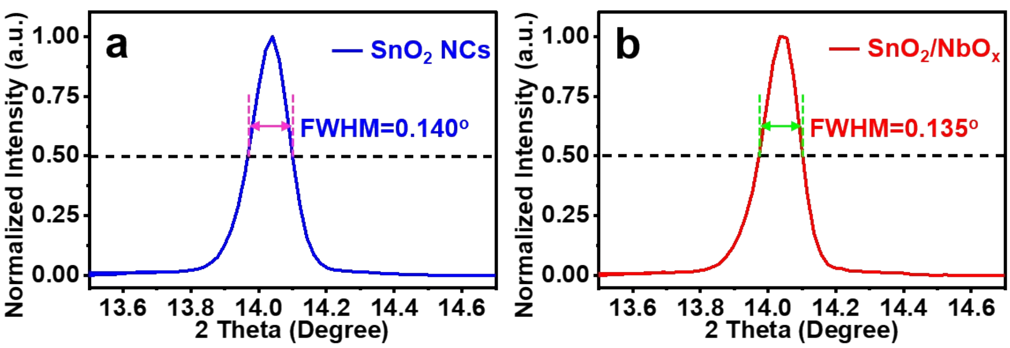

Figure S14. The full width at half maximum (FWHM) of (100) plane for perovskite films based on: (a) SnO_2 and (b) SnO_2/NbO_x NCs.

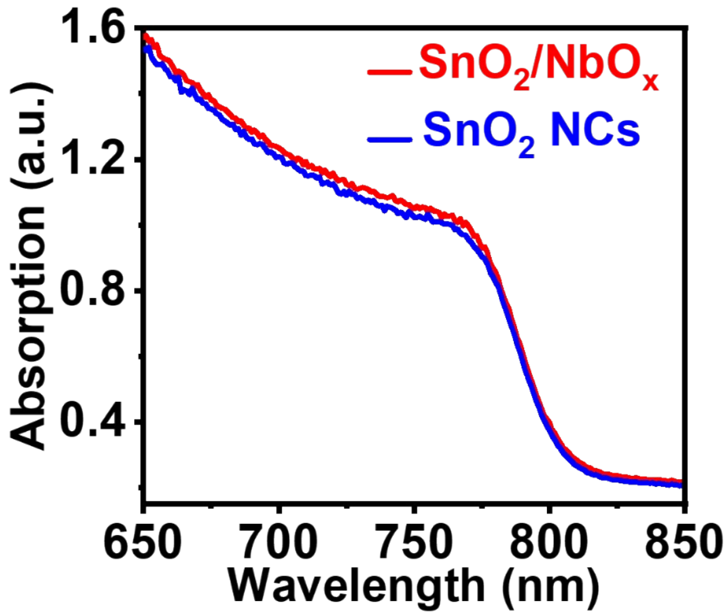

Figure S15. The UV-Vis absorption spectra of perovskite films on SnO_2 and SnO_2/NbO_x NC ETMs.

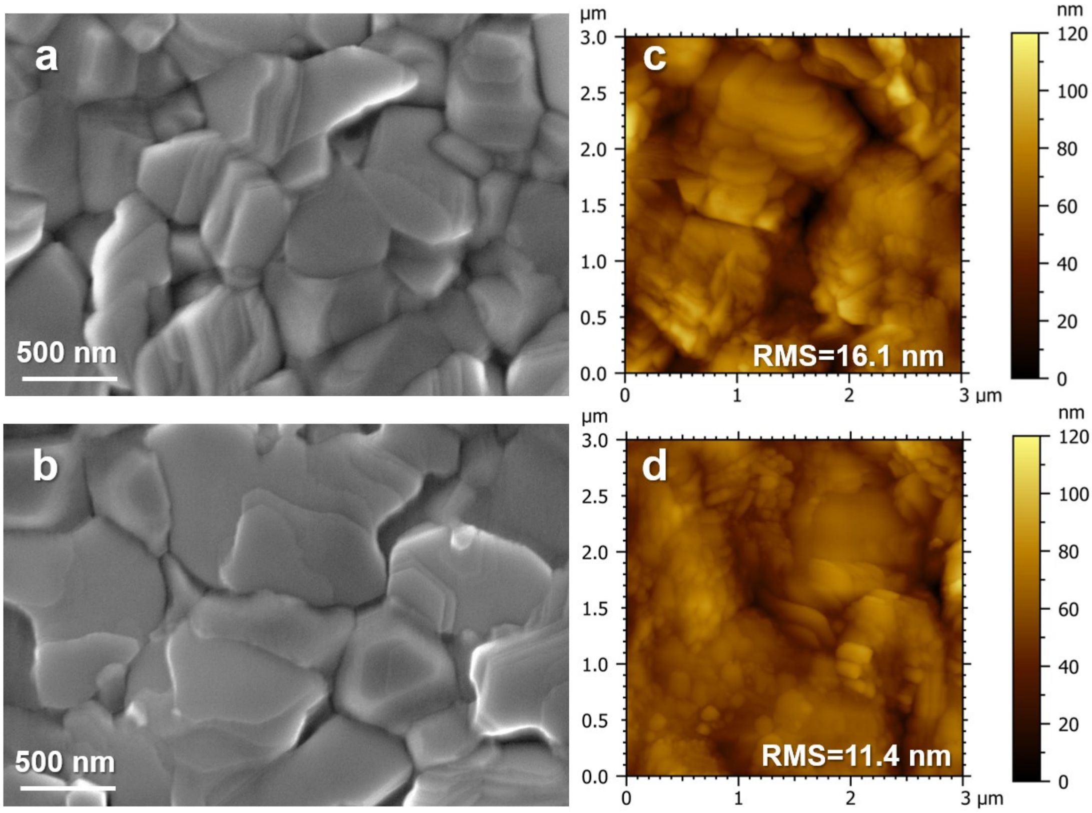

Figure S16. Morphologies of perovskite films on different ETMs: (a, c) SnO_2 and (b, d) SnO_2/NbO_x NCs.

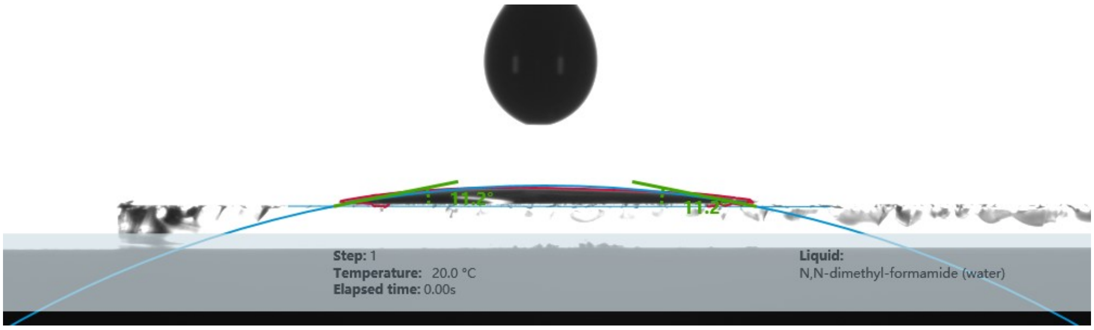

Figure S17. The contact angle of the PbI_2 solution on the commercial SnO_2 film.

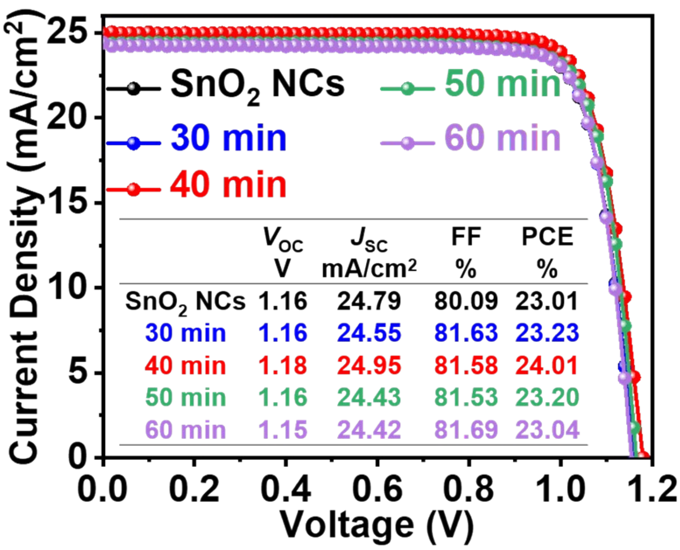

Figure S18. The *J-V* curves of devices based on SnO_2/NbO_x ETMs with different enveloping periods of NbO_x layer.

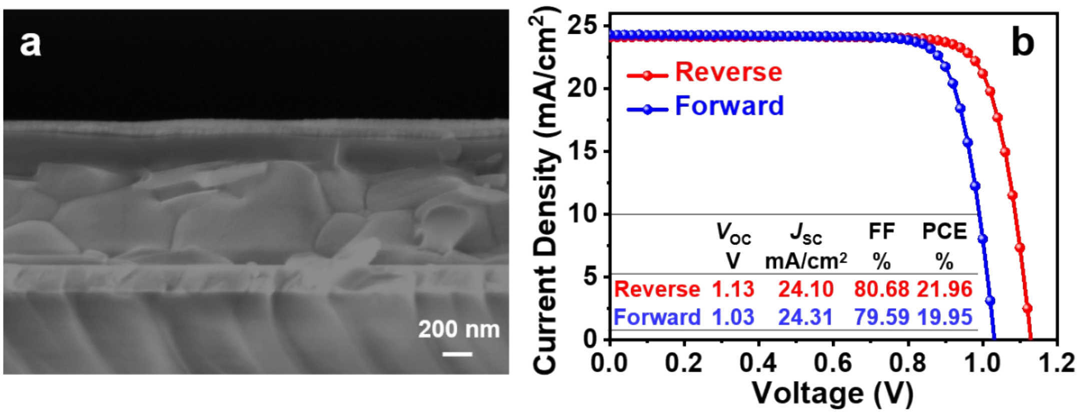

Figure S19. The characteristics of devices based on commercial SnO_2: (a) the cross-sectional SEM image of PSCs and (b) the *J-V* curves.

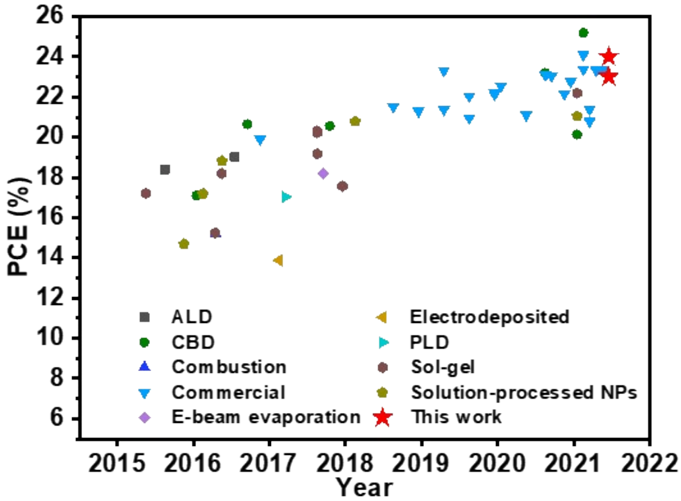

Figure S20. Schematic diagram of efficiency development of planar n-i-p PSCs based on SnO_2 ETMs.

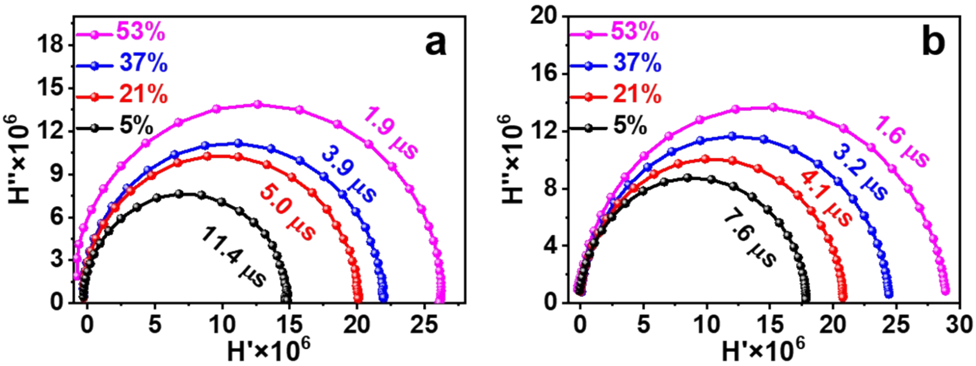

Figure S21. The IMPS spectra for devices based on different ETMs under different illumination intensity: (a) SnO_2 and (b) SnO_2/NbO_x NCs.

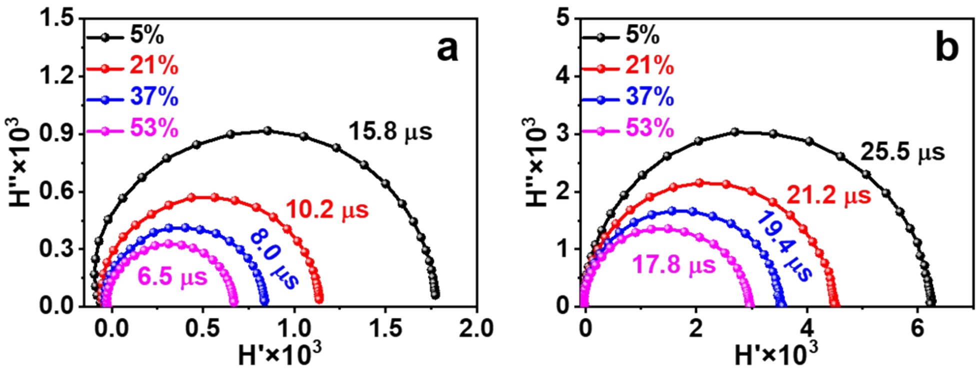

Figure S22. The IMVS spectra for devices on different ETMs under different illumination intensity: (a) SnO_2 and (b) SnO_2/NbO_x NCs.

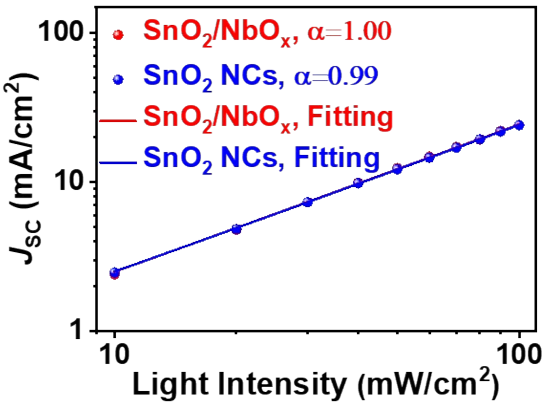

Figure S23. The relationship between J_{SC} versus light intensity for devices based on SnO_2 and SnO_2/NbO_x NCs.

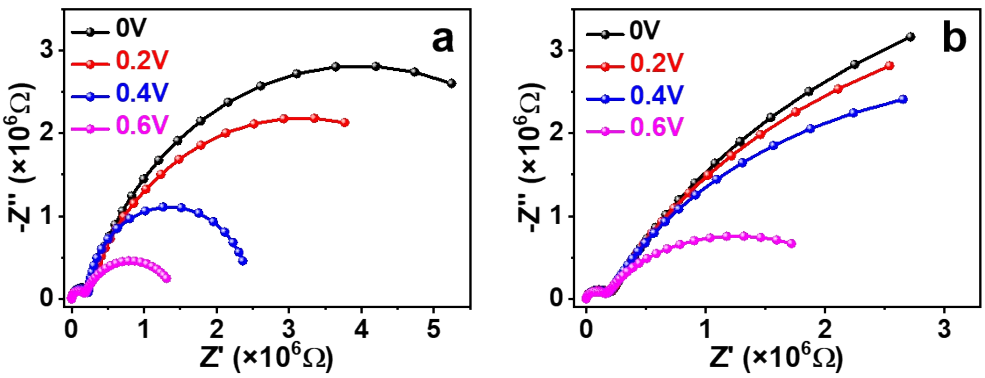

Figure S24. The Nyquist plots of different V_{bias} for devices based on different ETMs: (a) SnO_2 and (b) SnO_2/NbO_x NCs.

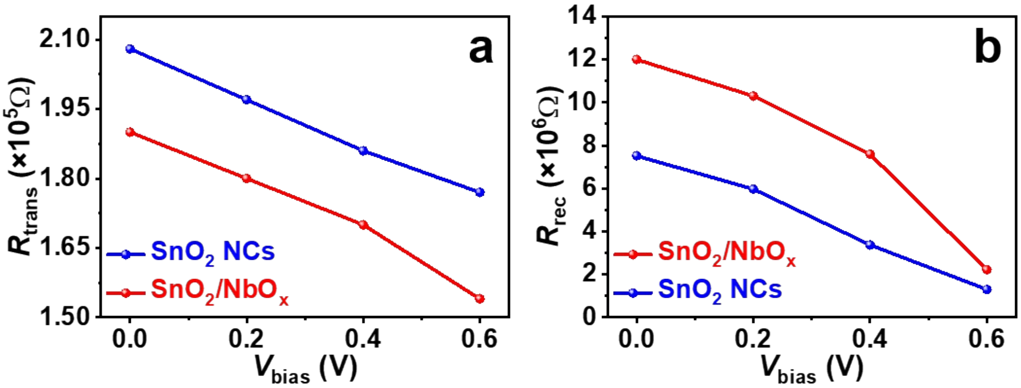

Figure S25. The relationship between resistance values (fitted from EIS in **Figure S18**) versus V_{bias} for devices based on SnO_2 and SnO_2/NbO_x NC ETMs: (a) R_{trans} and (b) R_{rec}.

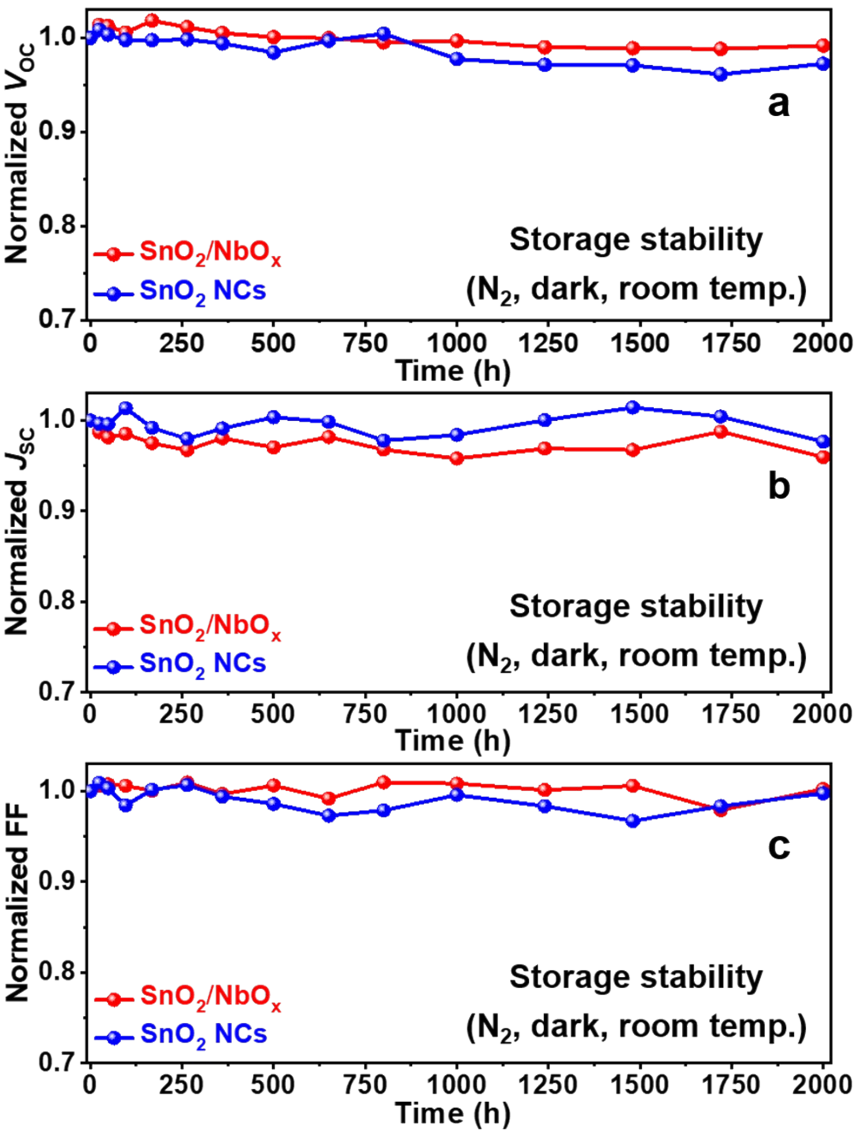

Figure S26. The normalized V_{OC}, J_{SC}, and FF as a function of aging times of long-term storage stability.

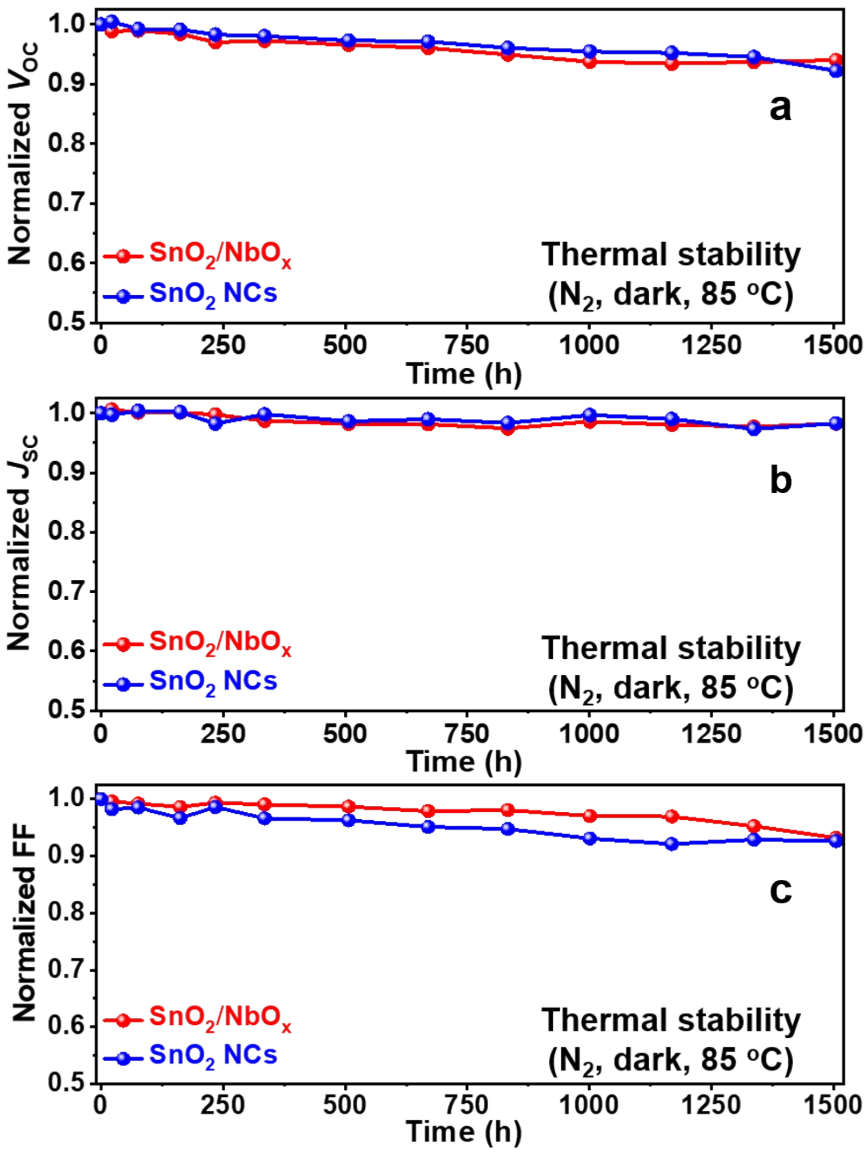

Figure S27. The normalized V_{OC}, J_{SC}, and FF as a function of aging times of thermal stability.

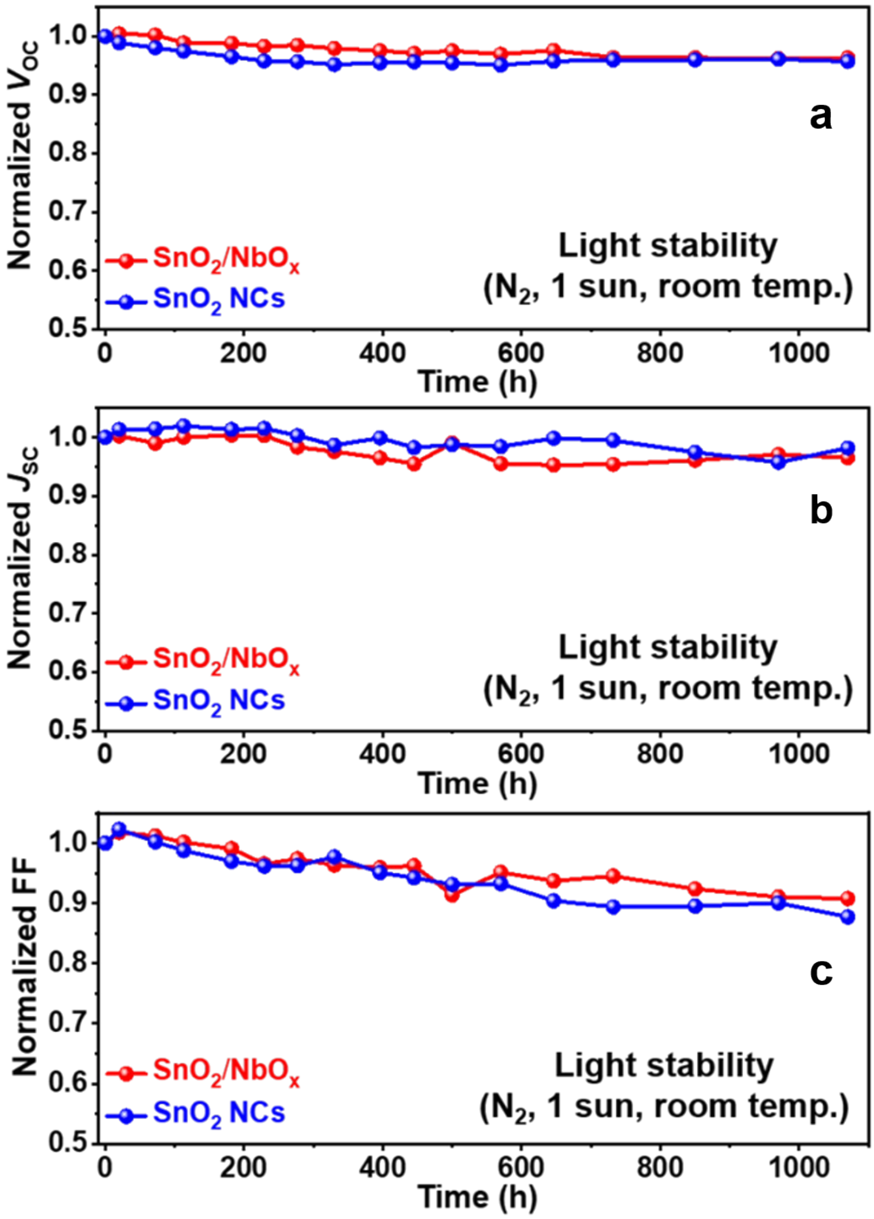

Figure S28. The normalized V_{OC}, J_{SC}, and FF as a function of aging times of light soaking stability.

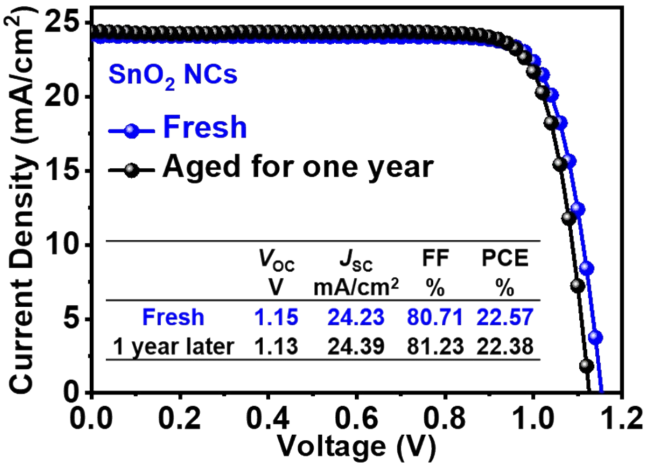

Figure S29. The *J*-*V* curves of devices based on fresh and aged dispersion solutions of SnO_2 NCs.

Table S1. The atomic ratio of SnO_2 and SnO_2/NbO_x NCs based on XPS survey spectrum in **Figure S7**.

Atomic (%)	Cl 2p	Sn 3d	Nb 3d	O 1s	C 1s
SnO_2 NCs	1.00	11.26	0.27	39.22	47.53
SnO_2/NbO_x NCs	1.28	8.25	7.22	45.07	33.35

Table S2. The characteristic properties of SnO_2 and SnO_2/NbO_x NCs films based in **Figure 3b-f**.

Method	*I-V*	SCLC			Mott-Schottky	
Device Structure	ITO/SnO_2/Au	ITO/SnO_2/PCBM/Au			ITO/ SnO_2	
	σ_0 (mS/cm)	μ (cm^2/V·s)	V_{TFL} (V)	N_t (cm^{-3})	V_{fb} (V)	N_d (cm^{-3})
SnO_2 NCs	1.03×10^{-2}	1.80×10^{-3}	0.68	7.5×10^{17}	-1.64	9.6×10^{21}
SnO_2/NbO_x NCs	1.23×10^{-2}	2.27×10^{-3}	0.51	5.6×10^{17}	-1.62	1.4×10^{22}

Table S3. Device performance and detailed parameters of planar n-i-p PSCs based on SnO_2 ETMs in **Figure S20**.

Deposition method	Device structure	J_{SC} mA/cm^2	V_{OC} V	FF %	PCE %	Year	Ref.
ALD	FTO/SnO_2/$(FAPbI_3)_{0.85}(MAPbBr_3)_{0.15}$/Spiro-OMeTAD/Au	21.3	1.14	74	18.4	2015	3
ALD	FTO/SnO_2/C60-SAM/$MAPbI_3$/Spiro-OMeTAD/Au	21.56	1.13	78.11	19.03	2016	4
CBD	FTO/SnO_2/PCBM/$FA_{0.83}Cs_{0.17}Pb(I_{0.6}Br_{0.4})_3$/Spiro-OMeTAD/Ag	19.4	1.2	75.1	17.1	2016	5
CBD	FTO/SnO_2/$K_x(Cs_{0.5}(FAMA)_{0.95})_{1-x}Pb(I_{0.85}Br_{0.15})_3$/Spiro-OMeTAD/Au	22.95	1.13	79	20.56	2017	6
CBD	FTO/SnO_2/$Cs_x(MA_{0.17}FA_{0.83})_{1-x}Pb(I_{0.83}Br_{0.17})_3$/Spiro-OMeTAD/Au	22.73	1.18	77	20.65	2016	7
CBD	ITO/SnO_2/$(FAPbI_3)_{1-x}(MAPbBr_3)_x$/Spiro-OMeTAD/Au	25.14	1.18	84.8	25.2	2021	8
CBD	FTO/SnO_2-NH_4F/$(FAPbI_3)_{0.95}(MAPbBr_3)_{0.05}$/Spir	24.6	1.16	81.4	23.2	2020	9

	o-OMeTAD/Au						
CBD	FTO/Eu:SnO_2/$MAPbI_3$/Spiro-OMeTAD/Au	22.6	1.13	78.76	20.14	2021	[10]
Combustion	ITO/SnO_2/C_{60}-SAM/$MAPbI_3$/Spiro-OMeTAD/Ag	21.53	1.07	65	15.18	2016	[11]
Commercial	ITO/SnO_2/$(FAPbI_3)_{0.97}(MAPbBr_3)_{0.03}$/Spiro-OMeTAD/Au	24.88	1.09	75.73	19.9	2016	[12]
Commercial	ITO/SnO_2/$FA_{1-x}MA_xPbI_3$/Spiro-OMeTAD/Au	25.2	1.18	78.4	23.32	2019	[2]
Commercial	ITO/SnO_2-$CoCl_2$/$(FAPbI_3)_{1-x}(MAPbBr_3)_x$/Spiro-OMeTAD/Au	24.57	1.2	79.52	23.37	2021	[13]
Commercial	ITO/SnO_2-MQDs/$FA_{0.9}MA_{0.05}Cs_{0.05}PbI_{0.98}Br_{0.02}$/Spiro-OMeTAD/$MoO_3$/Au	24.96	1.17	79.8	23.34	2021	[14]
Commercial	FTO/SnO_2-ImAcHCl/$(FAPbI_3)_{0.95}(MAPbBr_3)_{0.05}$/Spiro-OMeTAD/Au	23.06	1.15	79	20.96	2019	[15]
Commercial	ITO/SnO_2-RCQs/$Cs_{0.05}FA_{0.81}MA_{0.14}PbI_{2.55}Br_{0.45}$/Spiro-OMeTAD/$MoO_3$/Au	24.1	1.14	82.9	22.77	2020	[16]
Commercial	ITO/In_2O_3/SnO_2/$FA_{1-x}MA_xPbI_3$/Spiro-OMeTAD/Au	24.78	1.16	78.23	22.54	2020	[17]
Commercial	FTO/SnO_2-(g-CNQDs)/$Cs_x(MA_{0.15}FA_{0.85})_{1-x}Pb(I_{0.85}Br_{0.15})_3$/Spiro-OMeTAD/Au	24.03	1.18	78.3	22.13	2019	[18]
Commercial	ITO/SnO_2-NH_4Cl/$(FAPbI_3)_{0.97}(MAPbBr_3)_{0.03}$/Spiro-OMeTAD/Ag	24.25	1.14	76.75	21.38	2019	[19]
Commercial	ITO/SnO_2/B_2Cat_2/$Cs_{1-x-y}FA_xMA_yPbBr_zI_{1-z}$/Spiro-OMeTAD/Au	23.7	1.15	80.98	22.04	2019	[20]
Commercial	ITO/SnO_2-HP (heparin potassium) /$Cs_{0.05}FA_{0.85}MA_{0.10}Pb(I_{0.97}Br_{0.03})_3$/Spiro-OMeTAD/Au	24.97	1.16	79.4	23.06	2020	[21]
Commercial	ITO/SnO_2/KPF6/$Rb_{0.05}(FA_{0.95}MA_{0.05})_{0.95}PbI_{2.85}Br_{0.15}$/Spiro-OMeTAD/Au	22.83	1.14	81.8	21.39	2021	[22]
Commercial	ITO/SnO_2-EDTA/$FA_{0.95}Cs_{0.05}PbI_3$/Spiro-OMeTAD/Au	24.46	1.11	79	21.52	2018	[23]
Commercial	ITO/SnO_2/C9 (fullerene derivative) /$(FAPbI_3)_x(MAPbBr_3)_{1-x}$/Spiro-OMeTAD/Au	24.1	1.12	78.9	21.3	2018	[24]
Commercial	ITO/SnO_2-GDY (Graphdiyne)/ $Cs_xMA_yFA_{1-x-y}PbI_zBr_{3-z}$/Spiro-OMeTAD/Au	23.32	1.14	79.62	21.11	2020	[25]

Commercial	ITO/SnO_2-KCl/$(FAPbI_3)_{0.95}(MAPbBr_3)_{0.05}$/Spiro-OMeTAD/Au	24.2	1.14	80.7	22.2	2019	[26]
Commercial	ITO/SnO_2/RbF/$(FAPbI_3)_{0.95}(MAPbBr_3)_{0.05}$/Spiro-OMeTAD/Au	24.32	1.21	79.29	23.38	2021	[27]
Commercial	ITO/SnO_2/$FAPbI_3$/Spiro-OMeTAD/Au	24.4	1.16	81.3	23.1	2020	[28]
Commercial	ITO/SnO_2/$FAPbI_3$/Spiro-OMeTAD/MoO_3/Au	25.34	1.17	81.36	24.1	2021	[29]
Commercial	ITO/H_2O_2-SnO_2/$(FAPbI_3)_{1-x}(MAPbBr_3)_x$/Spiro-OMeTAD/Au	24.22	1.16	78.96	22.15	2020	[30]
Commercial	FTO/ SnO_2-CdS QD /$MAPbI_3$/Spiro-OMeTAD/Ag	23.45	1.13	78.42	20.78	2021	[31]
E-beam evaporation	FTO/SnO_2/$Cs_{0.05}(MA_{0.17}FA_{0.83})_{0.95}Pb(I_{0.83}Br_{0.17})_3$/Spiro-OMeTAD/Au	22.75	1.09	73	18.2	2017	[32]
Electro-deposited	ITO/SnO_2/$MAPbI_3$/Spiro-OMeTAD/Ag	19.75	1.08	65	13.88	2017	[33]
PLD	FTO/SnO_2/PCBM/$MAPbI_3$/Spiro-OMeTAD/Au	21.6	1.11	71	17.03	2017	[34]
Sol-gel	FTO/SnO_2/$MAPbI_3$/Spiro-OMeTAD/Au	23.27	1.11	67	17.21	2015	[35]
Sol-gel	ITO/SnO_2/$MAPbI_3$/Spiro-OMeTAD/Au	21.74	1.15	80.9	20.23	2017	[36]
Sol-gel	FTO/SnO_2/$(FAPbI_3)_{0.85}(MAPbBr_3)_{0.15}$ /Spiro-OMeTAD/Au	22.54	1.15	74	19.18	2017	[37]
Sol-gel	FTO/Mg:SnO_2/$MAPbI_3$/Spiro-OMeTAD/Au	21.44	1.00	70.8	15.24	2016	[38]
Sol-gel	FTO/Nb:SnO_2/$MAPbI_3$/Spiro-OMeTAD/Au	22.36	1.08	72.7	17.57	2017	[39]
Sol-gel	FTO/Li:SnO_2/$MAPbI_3$/Spiro-OMeTAD/Au	23.27	1.1	70.7	18.2	2016	[40]
Sol-gel	ITO/SnO_2:GQDs/$MAPbI_3$/Spiro-OMeTAD/Au	23.05	1.13	77.8	20.31	2017	[41]
Sol-gel	FTO/SnO_2:FAI/$Cs_{0.04}(FA_{0.84}MA_{0.16})_{0.96}Pb(I_{0.84}Br_{0.16})_3$/Spiro-OMeTAD/Au	23.2	1.18	80.8	22.2	2021	[42]
Solution-processed NPs	FTO/SnO_2/$MAPbI_3$/Spiro-OMeTAD/Au	21.19	1.02	67.8	14.69	2015	[43]
Solution-processed NPs	FTO/SnO_2/$Cs_{0.05}(MA_{0.17}FA_{0.83})_{0.95}Pb(I_{0.83}Br_{0.17})_3$/Spiro-OMeTAD/Au	23.05	1.13	79.8	20.79	2018	[44]
Solution-processed NPs	ITO/Sb:SnO_2/$MAPbI_3$/Spiro-OMeTAD/Au	22.6	1.06	72	17.2	2016	[45]

Solution-processed NPs	FTO/SnO_2/KPF_6/$(CsI)_{0.04}(FAI)_{0.82}(PbI_2)_{0.86}(MAPbBr_3)_{0.14}$/Spiro-OMeTAD/Au	23.15	1.12	81.2	21.05	2021	[46]
This work	ITO/SnO_2/$FA_{1-x}MA_xPbI_{3-y}Cl_y$/Spiro-OMeTAD/Au	24.79	1.16	80.09	23.01	2021	This work
This work	ITO/SnO_2/NbO_x/$FA_{1-x}MA_xPbI_{3-y}Cl_y$/Spiro-OMeTAD/Au	24.95	1.18	81.58	24.01	2021	This work

Table S4. Parameters of the TRPL spectroscopy based on perovskite films spin-coated on different substrates in **Figure 5b**.

Substrate	y_0	τ_1 (ns)	A_1	τ_2 (ns)	A_2	τ_{ave} (ns)
glass	0.016	128.1	0.42	4725	0.51	2463
SnO_2 NCs	0.0029	95.5	0.38	332.5	0.74	297.0
SnO_2/NbO_x NCs	0.0016	65.8	0.59	363.7	0.58	249.7

Table S5. EIS fitting parameters of the devices based on SnO_2 and SnO_2/NbO_x NCs in **Figure 5f** and **Figure S24**.

	V_{bias} (V)	R_s (Ohm)	C_1 (F)	R_{tr} (Ohm)	C_2 (F)	R_{rec} (Ohm)
SnO_2 NCs	0	38.12	9.13×10^{-9}	2.08×10^{-5}	2.18×10^{-5}	7.52×10^{-6}
	0.2	44.28	8.77×10^{-9}	1.97×10^{-5}	3.28×10^{-5}	5.97×10^{-6}
	0.4	30.01	8.78×10^{-9}	1.86×10^{-5}	3.95×10^{-5}	3.37×10^{-6}
	0.6	37.02	8.63×10^{-9}	1.77×10^{-5}	4.79×10^{-5}	1.30×10^{-6}
SnO_2/NbO_x NCs	0	27.96	9.78×10^{-9}	1.90×10^{-5}	5.05×10^{-5}	1.20×10^{-6}
	0.2	27.67	1.03×10^{-9}	1.80×10^{-5}	5.45×10^{-5}	1.03×10^{-6}
	0.4	27.71	9.85×10^{-10}	1.70×10^{-5}	5.28×10^{-5}	7.59×10^{-6}
	0.6	27.84	9.91×10^{-9}	1.54×10^{-5}	6.00×10^{-5}	2.22×10^{-6}

References

1. B. Bob, T.-B. Song, C.-C. Chen, Z. Xu and Y. Yang, *Chem. Mater.*, 2013, **25**, 4725-4730.
2. Q. Jiang, Y. Zhao, X. W. Zhang, X. L. Yang, Y. Chen, Z. M. Chu, Q. F. Ye, X. X. Li, Z. G. Yin and J. B. You, *Nat. Photonics*, 2019, **13**, 460-466.
3. J. P. C. Baena, L. Steier, W. Tress, M. Saliba, S. Neutzner, T. Matsui, F. Giordano, T. J. Jacobsson, A. R. S. Kandada, S. M. Zakeeruddin, A. Petrozza, A. Abate, M. K. Nazeeruddin, M. Gratzel and A. Hagfeldt, *Energy Environ. Sci.*, 2015, **8**, 2928-2934.
4. C. L. Wang, D. W. Zhao, C. R. Grice, W. Q. Liao, Y. Yu, A. Cimaroli, N. Shrestha, P. J. Roland, J. Chen, Z. H. Yu, P. Liu, N. Cheng, R. J. Ellingson, X. Z. Zhao and Y. F. Yan, *J. Mater. Chem. A*, 2016, **4**, 12080-12087.
5. D. P. McMeekin, G. Sadoughi, W. Rehman, G. E. Eperon, M. Saliba, M. T. Horantner, A. Haghighirad, N. Sakai, L. Korte, B. Rech, M. B. Johnston, L. M. Herz and H. J. Snaith, *Science*, 2016, **351**, 151-155.
6. T. L. Bu, X. P. Liu, Y. Zhou, J. P. Yi, X. Huang, L. Luo, J. Y. Xiao, Z. L. Ku, Y. Peng, F. Z. Huang, Y. B. Cheng and J. Zhong, *Energy Environ. Sci.*, 2017, **10**, 2509-2515.
7. E. H. Anaraki, A. Kermanpur, L. Steier, K. Domanski, T. Matsui, W. Tress, M. Saliba, A. Abate, M. Gratzel, A. Hagfeldt and J. P. Correa-Baena, *Energy Environ. Sci.*, 2016, **9**, 3128-3134.
8. J. J. Yoo, G. Seo, M. R. Chua, T. G. Park, Y. L. Lu, F. Rotermund, Y. K. Kim, C. S. Moon, N. J. Jeon, J. P. Correa-Baena, V. Bulovic, S. S. Shin, M. G. Bawendi and J. Seo, *Nature*, 2021, **590**, 587-593.
9. E. H. Jung, B. Chen, K. Bertens, M. Vafaie, S. Teale, A. Proppe, Y. Hou, T. Zhu, C. Zheng and E. H. Sargent, *ACS Energy Lett.*, 2020, **5**, 2796-2801.
10. Y. L. Chen, X. J. Zuo, Y. Y. He, F. Qian, S. N. Zuo, Y. L. Zhang, L. Liang, Z. Q. Chen, K. Zhao, Z. K. Liu, J. Gou and S. Z. Liu, *Adv. Sci.*, 2021, **8**, 2001466.
11. X. Liu, K.-W. Tsai, Z. Zhu, Y. Sun, C.-C. Chueh and A. K. Y. Jen, *Adv. Mater. Interfaces*, 2016, **3**, 1600122.
12. Q. Jiang, L. Q. Zhang, H. L. Wang, X. L. Yang, J. H. Meng, H. Liu, Z. G. Yin, J. L. Wu, X. W. Zhang and J. B. You, *Nat. Energy*, 2017, **2**, 16177.
13. P. Wang, B. Chen, R. Li, S. Wang, N. Ren, Y. Li, S. Mazumdar, B. Shi, Y. Zhao and X. Zhang, *ACS Energy Lett.*, 2021, **6**, 2121-2128.
14. Y. G. Yang, H. Z. Lu, S. L. Feng, L. F. Yang, H. Dong, J. O. Wang, C. Tian, L. N. Li, H. L. Lu, J. Jeong, S. M. Zakeeruddin, Y. H. Liu, M. Gratzel and A. Hagfeldt, *Energy Environ. Sci.*, 2021, **14**, 3447-3454.
15. J. Chen, X. Zhao, S. G. Kim and N. G. Park, *Adv. Mater.*, 2019, **31**, 1902902.
16. W. Hui, Y. G. Yang, Q. Xu, H. Gu, S. L. Feng, Z. H. Su, M. R. Zhang, J. O. Wang, X. D. Li, J. F. Fang, F. Xia, Y. D. Xia, Y. H. Chen, X. Y. Gao and W. Huang, *Adv. Mater.*, 2020, **32**, 1906374.
17. P. Y. Wang, R. J. Li, B. B. Chen, F. H. Hou, J. Zhang, Y. Zhao and X. D. Zhang, *Adv. Mater.*, 2020, **32**, 1905766.
18. J. B. Chen, H. Dong, L. Zhang, J. R. Li, F. H. Jia, B. Jiao, J. Xu, X. Hou, J. Liu and Z. X. Wu, *J. Mater. Chem. A*, 2020, **8**, 2644-2653.
19. Z. Z. Liu, K. M. Deng, J. Hu and L. Li, *Angew. Chem. Int. Ed.*, 2019, **58**, 11497-11504.
20. N. Li, X. Niu, F. Pei, H. Liu, Y. Cao, Y. Liu, H. Xie, Y. Gao, Q. Chen, F. Mo and H. Zhou, *Sol. RRL*, 2020, **4**, 1900217.
21. S. You, H. Zeng, Z. Ku, X. Wang, Z. Wang, Y. Rong, Y. Zhao, X. Zheng, L. Luo, L. Li, S. Zhang, M. Li, X. Gao and X. Li, *Adv. Mater.*, 2020, **32**, 2003990.
22. H. Bi, B. Liu, D. He, L. Bai, W. Wang, Z. Zang and J. Chen, *Chem. Eng. J.*, 2021, **418**, 129375.
23. D. Yang, R. X. Yang, K. Wang, C. C. Wu, X. J. Zhu, J. S. Feng, X. D. Ren, G. J. Fang, S. Priya and S. Z. Liu, *Nat. Commun.*, 2018, **9**, 3239.
24. K. Liu, S. Chen, J. H. Wu, H. Y. Zhang, M. C. Qin, X. H. Lu, Y. F. Tu, Q. B. Meng and X. W. Zhan, *Energy Environ. Sci.*, 2018, **11**, 3463-3471.

25. S. Zhang, H. Si, W. Fan, M. Shi, M. Li, C. Xu, Z. Zhang, Q. Liao, A. Sattar, Z. Kang and Y. Zhang, *Angew. Chem. Int. Ed.*, 2020, **59**, 11573-11582.
26. P. Zhu, S. Gu, X. Luo, Y. Gao, S. Li, J. Zhu and H. Tan, *Adv. Energy Mater.*, 2020, **10**, 1903083.
27. J. Zhuang, P. Mao, Y. Luan, N. Chen, X. Cao, G. Niu, F. Jia, F. Wang, S. Cao and J. Wang, *Adv. Funct. Mater.*, 2021, **31**, 2010385.
28. H. Lu, Y. Liu, P. Ahlawat, A. Mishra, W. R. Tress, F. T. Eickemeyer, Y. Yang, F. Fu, Z. Wang, C. E. Avalos, B. I. Carlsen, A. Agarwalla, X. Zhang, X. Li, Y. Zhan, S. M. Zakeeruddin, L. Emsley, U. Rothlisberger, L. Zheng, A. Hagfeldt and M. Grätzel, *Science*, 2020, **370**, eabb8985.
29. W. Hui, L. F. Chao, H. Lu, F. Xia, Q. Wei, Z. H. Su, T. T. Niu, L. Tao, B. Du, D. L. Li, Y. Wang, H. Dong, S. W. Zuo, B. X. Li, W. Shi, X. Q. Ran, P. Li, H. Zhang, Z. B. Wu, C. X. Ran, L. Song, G. C. Xing, X. Y. Gao, J. Zhang, Y. D. Xia, Y. H. Chen and W. Huang, *Science*, 2021, **371**, 1359-1364.
30. H. B. Wang, H. G. Liu, F. H. Ye, Z. L. Chen, J. J. Ma, J. W. Liang, X. L. Zheng, C. Tao and G. J. Fang, *J. Power Sources*, 2021, **481**, 229160.
31. Z. Lv, L. He, H. P. Jiang, X. J. Ma, F. Y. Wang, L. Fan, M. B. Wei, J. H. Yang, L. L. Yang and N. N. Yang, *ACS Appl. Mater. Interfaces*, 2021, **13**, 16326-16335.
32. J. Ma, X. Zheng, H. Lei, W. Ke, C. Chen, Z. Chen, G. Yang and G. Fang, *Sol. RRL*, 2017, **1**, 1700118.
33. J.-Y. Chen, C.-C. Chueh, Z. Zhu, W.-C. Chen and A. K. Y. Jen, *Sol. Energy Mater Sol. Cells*, 2017, **164**, 47-55.
34. Z. Chen, G. Yang, X. Zheng, H. Lei, C. Chen, J. Ma, H. Wang and G. Fang, *J. Power Sources*, 2017, **351**, 123-129.
35. W. J. Ke, G. J. Fang, Q. Liu, L. B. Xiong, P. L. Qin, H. Tao, J. Wang, H. W. Lei, B. R. Li, J. W. Wan, G. Yang and Y. F. Yan, *J. Am. Chem. Soc.*, 2015, **137**, 6730-6733.
36. L. Zuo, H. Guo, D. W. deQuilettes, S. Jariwala, N. De Marco, S. Dong, R. DeBlock, D. S. Ginger, B. Dunn, M. Wang and Y. Yang, *Sci. Adv.*, 2017, **3**, e1700106.
37. Q. Dong, Y. Shi, C. Zhang, Y. Wu and L. Wang, *Nano Energy*, 2017, **40**, 336-344.
38. L. B. Xiong, M. C. Qin, G. Yang, Y. X. Guo, H. W. Lei, Q. Liu, W. J. Ke, H. Tao, P. L. Qin, S. Z. Li, H. Q. Yu and G. J. Fang, *J. Mater. Chem. A*, 2016, **4**, 8374-8383.
39. X. D. Ren, D. Yang, Z. Yang, J. S. Feng, X. J. Zhu, J. Z. Niu, Y. C. Liu, W. G. Zhao and S. F. Liu, *ACS Appl. Mater. Interfaces*, 2017, **9**, 2421-2429.
40. M. Park, J. Y. Kim, H. J. Son, C. H. Lee, S. S. Jang and M. J. Ko, *Nano Energy*, 2016, **26**, 208-215.
41. J. S. Xie, K. Huang, X. G. Yu, Z. R. Yang, K. Xiao, Y. P. Qiang, X. D. Zhu, L. B. Xu, P. Wang, C. Cui and D. R. Yang, *ACS Nano*, 2017, **11**, 9176-9182.
42. Q. S. Dong, C. Zhu, M. Chen, C. Jiang, J. Y. Guo, Y. L. Feng, Z. H. Dai, S. K. Yadavalli, M. Y. Hu, X. Cao, Y. Q. Li, Y. Z. Huang, Z. Liu, Y. T. Shi, L. D. Wang, N. P. Padture and Y. Y. Zhou, *Nat. Commun.*, 2021, **12**, 973.
43. H. S. Rao, B. X. Chen, W. G. Li, Y. F. Xu, H. Y. Chen, D. B. Kuang and C. Y. Su, *Adv. Funct. Mater.*, 2015, **25**, 7200-7207.
44. G. Yang, C. Chen, F. Yao, Z. L. Chen, Q. Zhang, X. L. Zheng, J. J. Ma, H. W. Lei, P. L. Qin, L. B. Xiong, W. J. Ke, G. Li, Y. F. Yan and G. J. Fang, *Adv. Mater.*, 2018, **30**, 1706023.
45. A. Agresti, S. Pescetelli, L. Cina, D. Konios, G. Kakavelakis, E. Kymakis and A. Di Carlo, *Adv. Funct. Mater.*, 2016, **26**, 2686-2694.
46. Z. C. Wang, T. Wu, L. Xiao, P. L. Qin, X. L. Yu, L. Ma, L. Xiong, H. X. Li, X. B. Chen, Z. Wang, T. Wu, L. Xiao, P. Qin, X. Yu, L. Ma, L. Xiong, H. Li and X. Chen, *J. Power Sources*, 2021, **488**, 229451.